Applied Catalysis A: General 467 (2013) 154–162

Contents lists available at ScienceDirect

Applied Catalysis A: General

journal homepage: www.elsevier.com/locate/apcata

Amination of allyl alcohol to propionitrile over a $Zn_{30}Cr_{4.5}/\gamma$-Al_2O_3 bimetallic catalyst via coupled dehydrogenation–hydrogenation reactions

Yuecheng Zhang, Tianyu Wei, Yanjie Pian, Jiquan Zhao *

School of Chemical Engineering and Technology, Hebei University of Technology, Tianjin 300130, PR China

ARTICLE INFO

Article history:
Received 11 April 2013
Received in revised form 5 July 2013
Accepted 11 July 2013
Available online 20 July 2013

Keywords:
Allyl alcohol
Amination
Propionitrile
Bimetallic catalyst
$Zn_{30}Cr_{4.5}/\gamma$-Al_2O_3

ABSTRACT

A $Zn_{30}Cr_{4.5}/\gamma$-Al_2O_3 bimetallic catalyst that can perform coupled dehydrogenation and hydrogenation reactions was prepared for the amination of allyl alcohol to propionitrile. During the catalysis, the hydrogen derived from the dehydrogenation of the alcohol and imine acted as an in situ source for the hydrogenation of the carbon-carbon double bond. The catalyst exhibited good performance for the reaction at atmospheric ammonia pressure. The parameters that affect the catalyst performance were studied thoroughly, and an optimized process for synthesizing propionitrile from allyl alcohol and ammonia over the catalyst was obtained. Under the optimized conditions, the propionitrile yield was greater than 65%. The characterization results indicated that the dehydrogenation reaction mainly occurred on the Lewis acid sites and revealed that $ZnAl_2O_4$ is the active species for the coupled dehydrogenation–hydrogenation reactions. Chromium doping of the γ-Al_2O_3-supported zinc catalyst Zn_{30}/γ-Al_2O_3 resulted in a decrease in the size of the $ZnAl_2O_4$ crystallites, which was favorable for the dehydrogenation–hydrogenation reactions. The characterization results also revealed that the catalyst deactivation was due to carbon deposition on the catalyst during the catalytic run. The catalyst could be reactivated by blowing air into the reactor at a high temperature.

1. Introduction

In organic synthesis, nitriles are important intermediates that can easily be converted into a variety of compounds [1]. Low-molecular-weight aliphatic nitriles, such as acetonitrile, are used as solvents. Aliphatic nitriles can be obtained from the amination-dehydrogenation of alcohols [2,3]. In this process, two moles of hydrogen are released, as shown in Eq. (1):

$$RCH_2OH + NH_3 \rightarrow RCN + H_2O + 2H_2 \quad (1)$$

Recently, we successfully synthesized acetonitrile through the amination-dehydrogenation of ethanol over a $CoNi/\gamma$-Al_2O_3 catalyst [4–6]. Analysis of the results showed that pyridine bases and butyronitrile were formed in addition to acetonitrile. Pyridine bases are common by-products in the synthesis of acetonitrile from ethanol [7] or acetaldehyde [8]. However, the detection of butyronitrile with a selectivity as high as 7.6% under certain conditions was unexpected. We proposed that butyronitrile is formed as shown in Scheme 1[5]. First, ethanol is dehydrogenated to acetaldehyde. Then two molecules of acetaldehyde undergo aldol condensation on the acid sites of the catalyst to give crotonaldehyde. After the formation of crotonaldehyde, there are two possible pathways (A and B) to produce butyronitrile from crotonaldehyde. In path A, crotonaldehyde condenses with ammonia to generate the intermediate imine. Then the imine is dehydrogenated to give crotonitrile and hydrogen. Lastly, the carbon-carbon double bond in the crotonitrile molecule is hydrogenated with the hydrogen generated from the dehydrogenation of the imine and alcohol to give butyronitrile. In path B, the hydrogenation of crotonaldehyde occurs first to give butyroaldehyde. Then butyroaldehyde condenses with ammonia, and dehydrogenation follows to give butyronitrile. The results indicated that the hydrogen generated in situ can serve as a hydrogen source for the hydrogenation of unsaturated compounds in the transformation of crotonaldehyde to butyronitrile. The interesting results motivated us to find an effective catalyst with the capacity to perform dehydrogenation–hydrogenation reactions using the hydrogen generated in situ. The amination of allyl alcohol to propionitrile was used as a model reaction, and a series of catalysts were tested. Interestingly, the dehydrogenation–hydrogenation coupling was successful; yet, 3-methyl pyridine was obtained as a major by-product. Herein, we report the preliminary results.

* Corresponding author. Tel.: +86 22 60202926; fax: +86 22 60202926.
E-mail address: zhaojq@hebut.edu.cn (J. Zhao).

0926-860X/$ – see front matter © 2013 Elsevier B.V. All rights reserved.
http://dx.doi.org/10.1016/j.apcata.2013.07.026

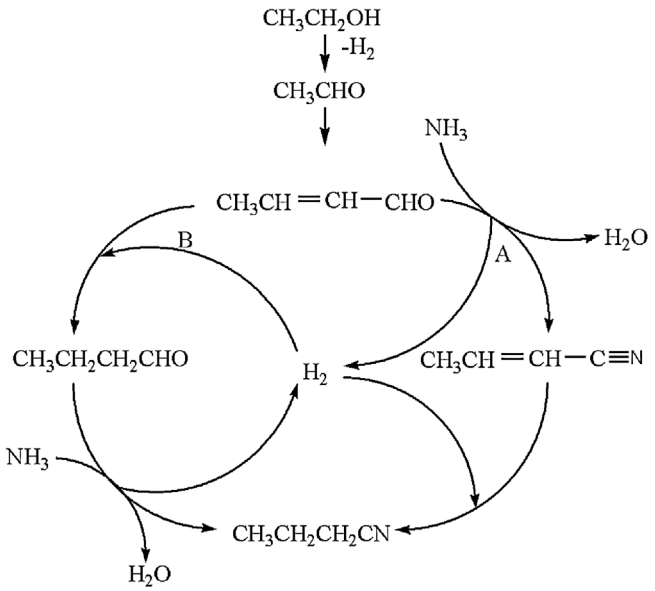

Scheme 1. Pathway for the formation of butyronitrile from ethanol.

2. Experimental

2.1. Catalyst preparation

All the chemicals were reagent grade. The zeolite and calcium bentonite were purchased from Nankai University Catalyst Plant, Tianjin, China. γ-Al_2O_3, ZrO_2 and SiO_2 were purchased from Tianjin Research and Design Institute of Chemical Industry, Tianjin, China. The supported metal oxide catalysts were prepared by kneading a mixture of γ-Al_2O_3 with an aqueous solution of the corresponding transition metal nitrates. These mixtures were then dried and calcined at 550 °C for 6 h. For example, the $Zn_{30}Cr_{4.5}$/γ-Al_2O_3 catalyst (the subscripts represent the zinc and chromium contents in the catalyst) was prepared as follows: 25.11 g of $Zn(NO_3)_2{\cdot}6H_2O$ and 6.34 g of $Cr(NO_3)_2{\cdot}6H_2O$ were dissolved in 5 g of water, and then 12.0 g of γ-Al_2O_3 was added to the solution. The mixture was then kneaded for 2 h in a kneader, and the resulting kneaded material was processed in an extruder to obtain extrudates with a diameter of 2 mm and length of 2.5 mm. The extrudates were dried at 110 °C for 6 h and then calcined at 550 °C for 6 h to yield the catalyst.

2.2. Catalyst characterization

To determine the metal content, the sample was first dissolved in concentrated HNO_3 and HF. Then the metal content of the solution was analyzed using a T.J.A. ICP-9000 (N + M) ICP-AES instrument. The XRD patterns of the samples were recorded with a Rigaku D/max 2500 X-ray diffractometer using Cu Kα radiation (40 kV, 150 mA) in the range of $2\theta = 10–90°$. X-ray photoelectron spectroscopy (XPS) was performed using a PHI 1600 spectrometer and Mg Kα X-ray excitation source. Transmission electron microscopy (TEM) was performed using a JEOL 100CX-II instrument. The specimens for TEM analysis were prepared by ultrasonic dispersion in *n*-butanol and subsequent evaporation of a drop of the resultant suspension on a lacey carbon/Cu grid. The surface area, total pore volume and pore size distribution of the samples were measured by nitrogen adsorption at 77 K using a Micromeritics ASAP 2020 surface area and porosity analyzer. The IR spectra of adsorbed pyridine were recorded on a Thermo Nicliet Nicolet Nexus 470 spectrometer equipped with a heatable and evacuatable IR cell with CaF_2 windows connected to a gas dosing-evacuation system. The powdered samples were pressed into self-supporting wafers with a diameter of 20 mm and weight of 50 mg. Prior to analysis, all samples were pretreated at 400 °C for 1 h under high vacuum conditions (5×10^{-5} Pa), followed by cooling to 200 °C. Then pyridine was adsorbed at this temperature for 15 min. The physisorbed pyridine was removed by evacuation at 200 °C under high vacuum conditions (5×10^{-5} Pa) for 1 h. Then the infrared spectra were recorded.

2.3. Catalytic tests

The catalytic amination of allyl alcohol to propionitrile was performed in a fixed-bed reactor with an internal diameter of 20 mm and length of 1000 mm. The fixed-bed reactor was placed in an electric furnace consisting of four heating zones equipped with four temperature controllers. In the experiments, 15 ml of the prepared solid catalyst was charged into the center of the reactor to avoid any temperature gradients, while the top and bottom of the reactor were filled with an inert packing material (Pyrex glass chips). The thermocouple was inserted in the center of the catalyst bed to monitor the temperature. The catalyst was reduced with hydrogen at 360 °C before the reaction. The controlled flows of ammonia and allyl alcohol were passed separately into a vaporizer in which the two reactants were preheated, vaporized and mixed perfectly. Then the mixed gas was fed into the catalyst bed. The reaction temperature was varied from 360 °C to 480 °C in approximately 30 °C steps. The products were collected in a condenser, and the tail gas of the reactor was fed successively into flasks filled with water to recover the low boiling point compounds and unreacted ammonia. The liquid products were separated in a gas–liquid separator and analyzed by a gas chromatograph equipped with a 30 m PEG-20M capillary column and thermal conductivity detector (TCD). H_2 was used as the carrier gas. The exhaust (H_2, NH_3, C_2H_4, etc.) was analyzed using the same gas chromatograph with N_2 as the carrier gas. All data were measured after the catalyst was on stream for 4 h. The selectivity was calculated using the peak area internal standard method. The components of the mixture were identified with a HP5971 MS equipped with a 30 m PEG-20M capillary column.

3. Results and discussion

3.1. Catalyst selection

The purpose of this work was to design a catalyst that catalyzes not only the dehydrogenation of alcohols and imines but also the hydrogenation of carbon-carbon double bonds with the hydrogen generated in situ from the dehydrogenation. It is well known that many supported transition metals can perform hydrogenation catalysis and some transition metals, such as zinc, nickel, etc., can catalyze the dehydrogenation of imines to nitriles in the amination of alcohols to nitriles [9,10]. Our previous studies showed that some Zn-based catalysts exhibit excellent performance in the dehydrogenation of imines in the amination of ethanol and styrene oxide to nitriles [4,5,9]. Initially, several catalysts containing 20% zinc were prepared on γ-Al_2O_3, H-ZSM-5, MCM-41, ZrO_2 and calcium bentonite. Their catalytic performances in the reaction of interest were tested, and the results are presented in Table 1. It was found that the allyl alcohol conversions over the catalysts supported on γ-Al_2O_3 and H-ZSM-5 were higher than 90% under atmospheric ammonia pressure at 693 K. However, the allyl alcohol conversions were very low in the cases of the ZrO_2 and calcium bentonite supports. The different activities of the catalysts might be due to the difference in the acidity of the support materials. GC–MS analysis indicated that the main components in the volatile products were propionitrile and 3-picoline. In addition, acetonitrile, isobutyronitrile and pyridine bases, including pyridine and 3,5-lutidine, were also detected.

Table 1
Performance of the zinc catalysts with different supports.

Catalyst	Conversion (%)	Selectivity (%)						
		PN	3-Pico	AN	Pyr	iso-BN	3,5-Luti	FD
Zn_{30}/SiO_2	82.7	18.9	14.7	3.9	2.5	5.7	0.7	0.7
Zn_{30}/calcium bentonite	36.6	0	28.2	6.5	11.3	0	5.2	0.6
Zn_{30}/ZrO_2	50.3	36.2	0	6.8	0	4.7	0	1.3
Zn_{30}/γ-Al_2O_3	94.4	46.5	8.9	2.1	2.4	2.8	2.2	1.6
Zn_{30}/H-ZSM-5	97.5	21.0	26.0	4.2	2.1	3.5	1.4	0.3

PN: propionitrile; 3-Pico: 3-picoline; AN: acetonitrile; Pyr: pyridine; iso-BN: *iso*-butyronitrile; 3,5-Luti: 3,5-lutidine; FD: formaldehyde.
Reaction conditions: reaction temperature 420 °C, ammonia/allyl alcohol molar ratio 3:1, atmospheric pressure, GHSV: 200 h^{-1}.

Table 2
Effect of the zinc content on the catalytic performance.

Catalyst	Conversion (%)	Selectivity (%)						
		PN	3-Pico	AN	Pyr	*iso*-BN	3, 5-Luti	FD
γ-Al_2O_3	98.6	4.5	17.5	0	1.1	0.7	6.2	1.4
Zn_{10}/γ-Al_2O_3	99.0	20.5	10.6	1.0	0.5	1.3	3.0	0.4
Zn_{20}/γ-Al_2O_3	99.0	23.5	9.4	0.6	2.5	2.6	4.0	0.7
Zn_{30}/γ-Al_2O_3	94.4	46.5	8.9	2.1	2.4	2.8	2.2	1.6
Zn_{40}/γ-Al_2O_3	92.6	6.9	2.4	0.4	1.7	0.05	0.7	1.8

PN: propionitrile; 3-Pico: 3-picoline; AN: acetonitrile; Pyr: pyridine; *iso*-BN: *iso*-butyronitrile; 3,5-Luti: 3,5-lutidine; FD: formaldehyde.
Reaction conditions: reaction temperature 420 °C, ammonia/allyl alcohol molar ratio 3:1, atmospheric pressure, GHSV 200 h^{-1}.

Of all the catalysts, the one on the γ-Al_2O_3 support had the highest conversion and selectivity in the coupled dehydrogenation–hydrogenation reactions. Therefore, the effect of the zinc content on the catalysis was studied in more detail to optimize the catalytic performance. A series of catalysts with different zinc contents was prepared and tested. The catalytic test results are given in Table 2. It can be seen that zinc is necessary for the transformation of allyl alcohol to propionitrile. The yield of the desired propionitrile product increased with increasing zinc content, reaching a maximum of 46.5% when the zinc content was 30%. Then it decreased sharply as the zinc content was further increased. When the zinc content was 40%, the propionitrile yield was only 6.9%. The yields of 3-picoline and 3,5-lutidine decreased monotonically as the zinc content was increased.

The Zn_{30}/γ-Al_2O_3 catalyst still did not give a satisfactory propionitrile yield. To improve the catalytic performance, Zn_{30}/γ-Al_2O_3 was doped with other metals, including Fe, Cu, Co, Ni and Cr, to prepare the corresponding bimetallic catalysts. The content of the second metal in all the bimetallic catalysts was 4.5%. The bimetallic catalysts were used in the amination of allyl alcohol to propionitrile, and the results are listed in Table 3.

It was found that the doping metals exhibited completely different effects on the catalyst. Co and Ni had no obvious effect on the catalytic performance, while Fe and Cu doping, especially the latter, led to a decrease in the propionitrile yield. However, the 3-picoline yield increased to some degree when the catalyst was doped with any of these four metals. Cr had a completely different effect on the catalyst than the other four metals. The Cr-doped catalyst exhibited better performance than the Zn_{30}/γ-Al_2O_3 catalyst. Specifically, doping Zn_{30}/γ-Al_2O_3 with Cr increased the propionitrile yield from 46.5% to 61.4%.

3.2. Performance of the $Zn_{30}Cr_{4.5}/\gamma$-Al_2O_3 catalyst under different reaction conditions

The influence of the reaction temperature on the performance of the $Zn_{30}Cr_{4.5}/\gamma$-Al_2O_3 catalyst was investigated in the temperature range of 633–753 K under atmospheric ammonia pressure, which was maintained with a molar ratio of ammonia to allyl alcohol of 3:1 and GHSV of 200 h^{-1}. The results shown in Table 4 indicated that the conversion of allyl alcohol increased with an increase in temperature. Meanwhile, the propionitrile yield increased with an increase in the temperature from 633 to 723 K and reached a maximum of 65.2% at 723 K. Above that temperature, the yield decreased with increasing temperature. It was also found that the yields of the acetonitrile and isobutyronitrile by-products increased with an increase in temperature. In contrast, the selectivity toward 3-picoline and other pyridine bases decreased with an increase in temperature. In principle, the formation of propionitrile competes with that of pyridines. Overall, high temperatures favored the formation of nitriles, but low temperatures favored the formation of pyridine bases in the experimental temperature range.

The influence of the molar ratio of ammonia to allyl alcohol on the reaction was investigated under atmospheric ammonia pressure and GHSV of 200 h^{-1} at 723 K. The results are presented in Table 4. As shown in the table, the propionitrile yield increased with

Table 3
Effect of the doped metals on the performance of the zinc-based catalyst.

Catalyst	Conversion (%)	Selectivity (%)						
		PN	3-Pico	AN	Pyr	*iso*-BN	3,5-Luti	FD
Zn_{30}/γ-Al_2O_3	94.4	46.5	8.9	2.1	2.4	2.8	2.2	1.6
$Zn_{30}Fe_{4.5}/\gamma$-Al_2O_3	98.0	43.1	14.0	2.2	1.1	2.0	0.7	0.5
$Zn_{30}Co_{4.5}/\gamma$-Al_2O_3	97.5	49.9	11.8	4.6	0.8	2.8	2.1	1.5
$Zn_{30}Cu_{4.5}/\gamma$-Al_2O_3	99.6	8.0	17.5	2.0	0.9	1.7	1.4	1.4
$Zn_{30}Ni_{4.5}/\gamma$-Al_2O_3	99.3	49.4	11.6	3.4	0.5	2.2	0.5	0.1
$Zn_{30}Cr_{4.5}/\gamma$-Al_2O_3	99.0	61.4	8.5	3.6	1.9	3.2	0.08	0.2

PN: propionitrile; 3-Pico: 3-picoline; AN: acetonitrile; Pyr: pyridine; *iso*-BN: *iso*-butyronitrile; 3,5-Luti: 3,5-lutidine; FD: formaldehyde.
Reaction conditions: reaction temperature 693 K, ammonia/allyl alcohol molar ratio 3:1, atmospheric pressure, GHSV 200 h^{-1}.

Table 4
Effect of the temperature on the performance of the $Zn_{30}Cr_{4.5}/\gamma\text{-}Al_2O_3$ catalyst.

Temperature (K)	Conversion (%)	Selectivity (%)						
		PN	3-Pico	AN	Pyr	*iso*-BN	3,5-Luti	FD
633	91.3	37.4	13.7	2.9	4.0	2.7	0.8	0.8
663	94.5	46.3	10. 9	5.8	2.5	2.6	0.7	0.8
693	99.0	61.4	8.6	3.7	2.0	3.3	0.1	0.3
723	99.0	65.2	7. 6	6.9	0.5	4.4	0.5	1.4
753	100	62.4	5.2	6.7	0.4	4.2	0.0	1.8

PN: propionitrile; 3-Pico: 3-picoline; AN: acetonitrile; Pyr: pyridine; iso-BN: *iso*-butyronitrile; 3,5-Luti: 3,5-lutidine; FD: formaldehyde.
Reaction conditions: ammonia/allyl alcohol molar ratio 3:1, atmospheric pressure, GHSV 200 h^{-1}.

Table 5
Effect of the molar ratio of ammonia to alcohol on the performance of the $Zn_{30}Cr_{4.5}/\gamma\text{-}Al_2O_3$ catalyst.

Ammonia/alcohol	Conversion (%)	Selectivity (%)						
		PN	3-Pico	AN	Pyr	*iso*-BN	3,5-Luti	FD
1:1	97.2	50.2	7.2	6.0	0.5	5.0	0.4	0.04
1:3	99.1	65.2	7. 6	6.9	0.4	4.4	0.5	1.4
1:6	100	58.4	7.4	8.1	0.3	2.3	0.3	0.3
1:12	100	57.7	2.4	9.7	0.3	0.5	0.2	0.7

PN: propionitrile; 3-Pico: 3-picoline; AN: acetonitrile; Pyr: pyridine; iso-BN: *iso*-butyronitrile; 3,5-Luti: 3,5-lutidine; FD: formaldehyde.
Reaction conditions: reaction temperature 420 °C, atmospheric pressure, GHSV: 200 h^{-1}.

an increase in the molar ratio of ammonia to allyl alcohol from 1:1 to 3:1 and reached a maximum of 65.2% at a ratio of 3:1. The yield then decreased gradually with further increases in the molar ratio of ammonia to allyl alcohol. It was also found that the acetonitrile by-product yield increased with an increase in the molar ratio of ammonia to allyl alcohol and acetonitrile became the second major component of the reaction mixture when the molar ratio of ammonia to allyl alcohol was higher than 3:1. The 3-picoline yield did not change significantly when the molar ratio of ammonia to allyl alcohol increased from 1:1 to 6:1. In general, an excess of ammonia did not favor the desired reaction, possibly because the excess ammonia molecules adsorbed on the acid centers of the catalyst, weakening the acidity of the catalyst and consequently impeding the condensation of aldehydes with ammonia to form imines, a key step in the formation of nitriles as shown in Scheme 2 (Table 5).

Generally, GHSV is another very important parameter that must be considered for a catalytic reaction occurring in a fixed-bed reactor. Therefore, the influence of GHSV on the catalytic performance was evaluated under atmospheric ammonia pressure and a molar ratio of ammonia to allyl alcohol of 3:1 at 693 K. The results shown in Table 6 indicated that the product yields did not change significantly as GHSV was varied from 100 h^{-1} to 300 h^{-1}. However, when GHSV was increased above 400 h^{-1}, the conversion of allyl alcohol and propionitrile yield decreased considerably due to the short residence time of the reactants on the catalyst.

The lifetime and regeneration of $Zn_{30}Cr_{4.5}/\gamma\text{-}Al_2O_3$ on-line were investigated, and the results are shown in Table 7. The conversion of allyl alcohol was higher than 99%, and the selectivity toward propionitrile was approximately 65% within the first 12 h that the catalyst was on stream. Then both the conversion and selectivity decreased gradually; the conversion and selectivity dropped to 88.3 and 52.06%, respectively, after the catalyst was on stream for 48 h. The catalyst deactivation over time on stream was due to the formation of carbonaceous deposits inside the pores during the catalytic run, which was confirmed by the TEM-EDX analysis and will be described in detail below. The regeneration of the catalyst was performed by continuously blowing air (STP 250 ml min^{-1}) into the fixed-bed reactor at 723 K for 3 h on-line, and the reaction was run once again using the regenerated catalyst. It was observed that both the conversion of allyl alcohol and the selectivity toward propionitrile obtained with the regenerated catalyst were similar to those obtained with the fresh catalyst. The results indicated that the carbonaceous deposits were removed, allowing the active sites to be exposed to the reactants and, therefore, the performance of the catalyst to be recovered after air regeneration.

3.3. Pathways for product generation

The composition of the products was analyzed by GC–MS. The analysis results revealed that the collected product mixture was composed of propionitrile, 3-picoline, acetonitrile, isobutyronitrile, pyridine, 3,5-lutidine and formaldehyde. No amine was detected in the mixture. Based on the analysis results, organic reaction principles [10] and related literature [11–14], the possible pathways for the generation of the products are given in Scheme 2.

As shown in Scheme 2, allyl alcohol is first dehydrogenated to acrolein, a key intermediate in the reaction. After the formation of acrolein, there are two possible pathways that yield

Table 6
Effect of GHSV on the catalytic performance.

GHSV (h^{-1})	Conversion (%)	Selectivity (%)						
		PN	3-Pico	AN	Pyr	*iso*-BN	3,5-Luti	FD
100	100	66.0	7.5	7.2	0.3	3.3	0.6	0.1
200	100	65.8	7.3	9.0	0.5	4.1	0.4	0.2
300	99.5	66.4	6.1	8.2	0.4	4.5	0.5	0.1
400	93.9	58.3	7.8	5.8	0.5	3.2	0.4	0.2
500	91.2	52.0	7.1	8.4	0.1	1.4	0.5	0.2
600	89.6	45.9	3.4	3.4	0.5	1.8	0.1	0.3

PN: propionitrile; 3-Pico: 3-picoline; AN: acetonitrile; Pyr: pyridine; iso-BN: *iso*-butyronitrile; 3,5-Luti: 3,5-lutidine; FD: formaldehyde.
Reaction conditions: reaction temperature 693 K, ammonia/allyl alcohol molar ratio 3:1, atmospheric pressure.

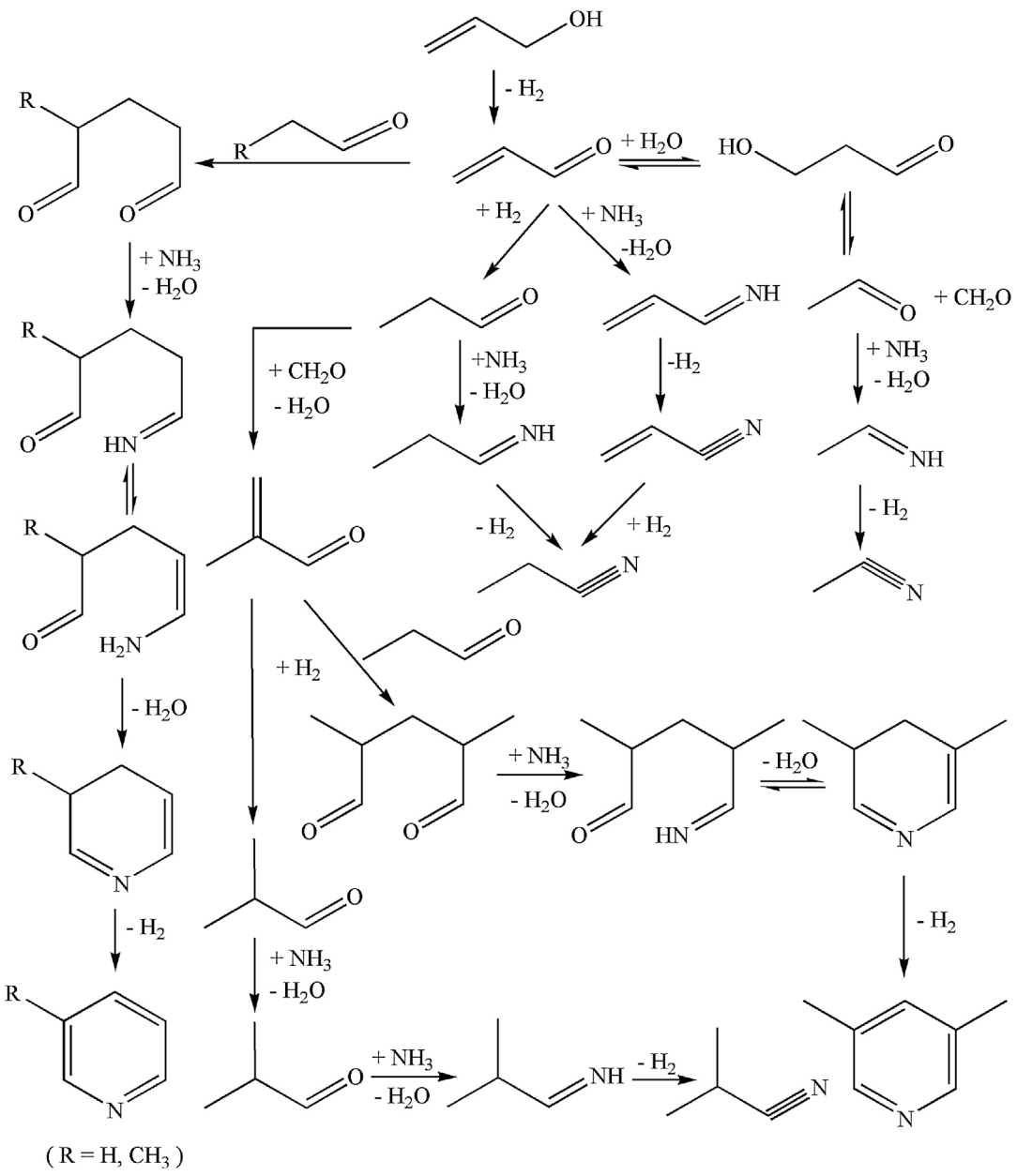

Scheme 2. Pathways for the product formation from the amination of allyl alcohol.

propionitrile similar to those for the formation of butyronitrile in the ethanol amination shown in Scheme 1. One is the condensation of acrolein with ammonia to give the intermediate imine, which is then dehydrogenated to generate acrylonitrile and hydrogen. Lastly, the carbon-carbon double bond in the acrylonitrile molecule is hydrogenated with the hydrogen generated from the dehydrogenation of the imine and alcohol to produce propionitrile. The other pathway involves the hydrogenation of acrolein

Table 7
Catalytic performance for different times on stream.

Time on steam (h)	Conversion (%)	Selectivity (%)						
		PN	3-Pico	AN	Pyr	*iso*-BN	3,5-Luti	FD
4	99.0	65.2	7. 6	6.9	0.5	4.4	0.5	1.4
12	100	65.5	6.5	6.5	0.6	5.7	0.9	0.9
24	98.3	57.8	8. 8	7.5	0.6	3.5	0.9	0.3
36	93.3	57.0	12.0	3.1	0.9	3.7	0.9	0.5
48	88.3	52.1	10.8	3.3	1.1	1.5	0.7	0.7
12[a]	99.7	65.2	9.1	4.6	1.0	4.3	0.5	1.0

PN: propionitrile; 3-Pico: 3-picoline; AN: acetonitrile; Pyr: pyridine; iso-BN: *iso*-butyronitrile; 3,5-Luti: 3,5-lutidine; FD: formaldehyde.
Reaction conditions: reaction temperature 420 °C, ammonia/allyl alcohol molar ratio 3:1, atmospheric pressure, GHSV 200 h^{-1}.
[a] Regenerated catalyst.

with the generated hydrogen to give propionaldehyde. Then the propionaldehyde condenses with ammonia and is dehydrogenated to give propionitrile. For the formation of acetonitrile, acrolein is first hydrated to generate 3-hydroxy propionaldehyde. Then 3-hydroxy propionaldehyde undergoes inverse aldol condensation to yield acetaldehyde and formaldehyde. The amination of acetaldehyde to give acetonitrile is described elsewhere [5]. The previously produced propionaldehyde can condense with formaldehyde to generate 2-methyl acrolein, which is hydrogenated to 2-methyl propionaldehyde. Then 2-methyl propionaldehyde reacts with ammonia to give isobutyronitrile, which is similar to the reaction for the formation of acetonitrile. The formation of pyridine bases occurs as described in the literature [11–13] and is not discussed here.

3.4. Catalyst characterization

To elucidate the active species and deactivation mechanism of the catalyst, the catalyst was characterized by XRD, XPS, TEM-EDX and N_2 adsorption–desorption, and IR spectra of adsorbed pyridine were collected. Fig. 1 shows the diffraction patterns of the fresh, used and regenerated $Zn_{30}Cr_{4.5}/\gamma\text{-}Al_2O_3$ samples, $Zn_{30}Cr_{4.5}/\gamma\text{-}Al_2O_3$ and $\gamma\text{-}Al_2O_3$. All the patterns except for that of $\gamma\text{-}Al_2O_3$ demonstrated the presence of a $ZnAl_2O_4$ crystalline phase [15–17]. No other crystalline phase was observed.

As reported in the literature [18–20], the heterogeneous $ZnAl_2O_4$ catalyst is active in many reactions, such as dehydration, hydrogenation, dehydrogenation, dehydrogenative condensation of normal alcohols, methylation of phenolic compounds and N-alkylation of 2-hydroxypyridine with methanol. It can therefore be concluded that $ZnAl_2O_4$ is the active species for the dehydrogenation–hydrogenation of the intermediate acrolein imine to propionitrile. It was observed that the $ZnAl_2O_4$ peaks of the fresh $Zn_{30}Cr_{4.5}/\gamma\text{-}Al_2O_3$ sample were weaker and broader than those of the $Zn_{30}/\gamma\text{-}Al_2O_3$ sample. In general, the full width at half maximum of the XRD peak is related to the particle size of crystal materials. The width increases as the size of the crystallites decreases. The average diameters of the $ZnAl_2O_4$ crystallites in $Zn_{30}/\gamma\text{-}Al_2O_3$ and $Zn_{30}Cr_{4.5}/\gamma\text{-}Al_2O_3$ calculated using the Scherrer formula were 5.2 nm and 7.1 nm, respectively. Therefore, the

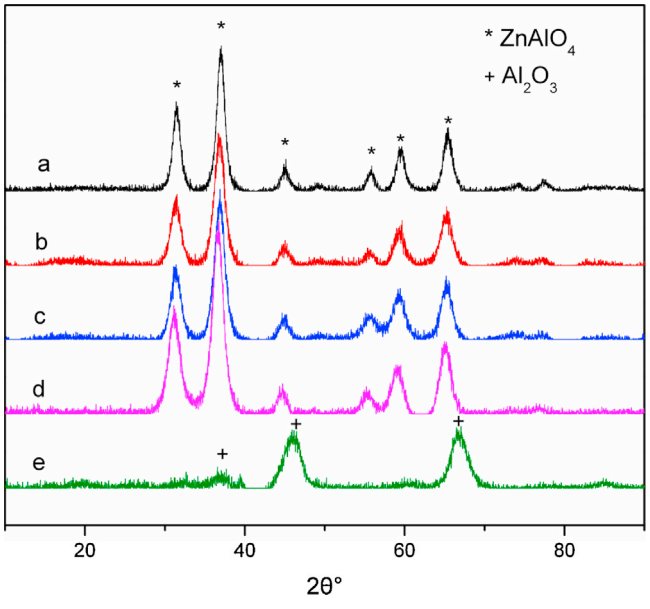

Fig. 1. XRD patterns of the catalyst samples. (a) $Zn_{30}/\gamma\text{-}Al_2O_3$; (b) $Zn_{30}Cr_{4.5}/\gamma\text{-}Al_2O_3$ (Fresh); (c) $Zn_{30}Cr_{4.5}/\gamma\text{-}Al_2O_3$ (Used); (d) $Zn_{30}Cr_{4.5}/\gamma\text{-}Al_2O_3$ (Regenerated); (e) $\gamma\text{-}Al_2O_3$.

Table 8
Textural properties of $Zn_{30}/\gamma\text{-}Al_2O_3$ and fresh, used and regenerated $Zn_{30}Cr_{4.5}/\gamma\text{-}Al_2O_3$.

Catalyst	S_{BET}[a] ($m^2\ g^{-1}$)	V[b] ($cm^3\ g^{-1}$)	d_p[c] (nm)
$Zn_{30}/\gamma\text{-}Al_2O_3$	99.61	0.316	12.68
$Zn_{30}Cr_{4.5}/\gamma\text{-}Al_2O_3$ (fresh)	99.86	0.268	8.89
$Zn_{30}Cr_{4.5}/\gamma\text{-}Al_2O_3$ (used)	54.16	0.129	9.51
$Zn_{30}Cr_{4.5}/\gamma\text{-}Al_2O_3$ (regenerated)	97.77	0.239	9.76

[a] BET surface area.
[b] BJH cumulative desorption pore volume.
[c] Mean pore diameter = $4\ V/S_{BET}$.

Cr doping of $Zn_{30}/\gamma\text{-}Al_2O_3$ decreased the size of the $ZnAl_2O_4$ crystallites. These results were confirmed by the TEM images (Fig. 2). $ZnAl_2O_4$ particles with diameters of 2–5 nm and 5–15 nm were observed as dark spots in the TEM images of $Zn_{30}Cr_{4.5}/\gamma\text{-}Al_2O_3$ and $Zn_{30}/\gamma\text{-}Al_2O_3$, respectively. These particles were dispersed on the $\gamma\text{-}Al_2O_3$ surface. Thus, both the XRD and TEM data supported the conclusion that the average $ZnAl_2O_4$ particle size was smaller on $Zn_{30}Cr_{4.5}/\gamma\text{-}Al_2O_3$ than on $Zn_{30}/\gamma\text{-}Al_2O_3$, suggesting that Cr doping can suppress the growth of $ZnAl_2O_4$ grains. A similar phenomenon in which Cr doping of supported ZnO decreased the ZnO grain size was reported in the literature [21]. The XRD and TEM characterization in combination with the catalytic test results indicated that the small $ZnAl_2O_4$ particle size was favorable for the reaction. Meanwhile, the diffraction patterns of the used and regenerated $Zn_{30}Cr_{4.5}/\gamma\text{-}Al_2O_3$ samples did not change at all compared to those of the fresh sample, which indicated that the $ZnAl_2O_4$ active species was stable during the catalysis and regeneration procedure. Therefore, the deactivation of the catalyst was not due to the decomposition or transformation of the $ZnAl_2O_4$ active species. Comparison of the TEM images of the fresh, used and regenerated $Zn_{30}Cr_{4.5}/\gamma\text{-}Al_2O_3$ samples showed that some substances covered the surface of the used samples. After regeneration by on-line combustion, the substances disappeared. Therefore, the deactivation of the catalyst can be attributed to the carbonaceous deposits generated by the chemical adsorption of alkaline substances during the catalytic run. The EDX analysis supported this conclusion with measured carbon contents of 23.6% and 46.6% at points 1 and 2, respectively, in Fig. 2e.

To strengthen this assumption, the porous structure of the catalyst was further analyzed with nitrogen adsorption experiments. Table 8 presents the specific surface areas and the range of the pore structural parameters of $Zn_{30}/\gamma\text{-}Al_2O_3$ and fresh, used and regenerated $Zn_{30}Cr_{4.5}/\gamma\text{-}Al_2O_3$. As expected, fresh $Zn_{30}Cr_{4.5}/\gamma\text{-}Al_2O_3$ had a slightly lower surface area than $Zn_{30}/\gamma\text{-}Al_2O_3$ due to the Cr doping. After the $Zn_{30}Cr_{4.5}/\gamma\text{-}Al_2O_3$ catalyst was on stream for 48 h, the surface area decreased from 99.15 $m^2\ g^{-1}$ to 54.16 $m^2\ g^{-1}$, corresponding to a decrease in the pore volume from 0.276 $cm^3\ g^{-1}$ to 0.129 $cm^3\ g^{-1}$. The nitrogen adsorption and EDX results both indicated that carbon was deposited in the catalyst pores. After regeneration, the surface area increased from 54.16 $m^2\ g^{-1}$ to 97.77 $m^2\ g^{-1}$, and the pore volume increased from 0.129 $cm^3\ g^{-1}$ to 0.239 $cm^3\ g^{-1}$, which indicated that the textural properties of the catalyst, and thus the catalytic performance, were largely recovered.

The XPS technique is much more sensitive than XRD for the analysis of surface oxides. Therefore, the surface compositions of the fresh, used and regenerated samples were determined by XPS. Figs. 3 and 4 show the analysis results. The results revealed that the Zn $2p_{3/2}$ binding energies of $Zn_{30}/\gamma\text{-}Al_2O_3$ and $Zn_{30}Cr_{4.5}/\gamma\text{-}Al_2O_3$ were 1022.16 and 1021.96 eV, respectively, indicating that Zn was present as $ZnAl_2O_4$ in the catalysts [22]. The Zn $2p_{3/2}$ binding energies of the used and regenerated $Zn_{30}Cr_{4.5}/\gamma\text{-}Al_2O_3$ samples were similar to that of the fresh one, indicating that the catalyst was stable during the catalytic run as also revealed by the XRD

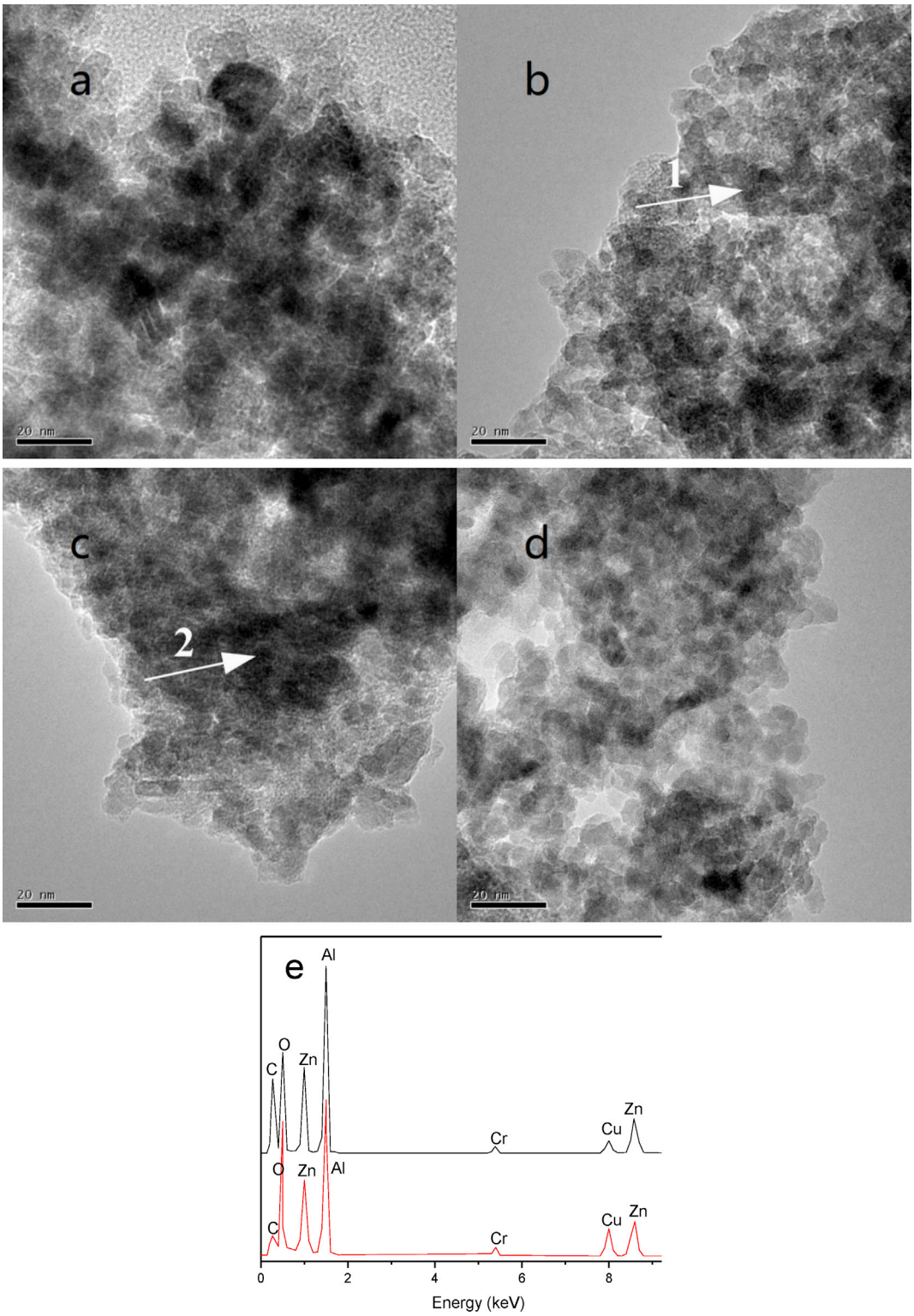

Fig. 2. TEM micrographs of the catalyst samples and EDX spectra at points 1 and 2. (a) $Zn_{30}/\gamma\text{-}Al_2O_3$; (b) $Zn_{30}Cr_{4.5}/\gamma\text{-}Al_2O_3$ (Fresh); (c) $Zn_{30}Cr_{4.5}/\gamma\text{-}Al_2O_3$ (Used); (d) $Zn_{30}Cr_{4.5}/\gamma\text{-}Al_2O_3$ (Regenerated); (e) EDX spectra at points 1 and 2.

analysis. In addition, the XPS spectra of the fresh, used and regenerated $Zn_{30}Cr_{4.5}/\gamma\text{-}Al_2O_3$ catalyst samples exhibited peaks near 577 eV corresponding to the Cr $2p_{3/2}$ binding energy. This binding energy revealed the presence of Cr^{3+}, most likely in the form of $ZnCr_2O_4$ [23].

The IR spectra of adsorbed pyridine were collected to determine the acidity of the $Zn_{30}/\gamma\text{-}Al_2O_3$ and fresh, used and regenerated $Zn_{30}Cr_{4.5}/\gamma\text{-}Al_2O_3$ catalysts. The results are shown in Fig. 5. A peak at 1450 cm^{-1} ascribed to pyridine adsorbed on Lewis acid sites [24–26] appeared in the spectra of $Zn_{30}/\gamma\text{-}Al_2O_3$ and the fresh $Zn_{30}Cr_{4.5}/\gamma\text{-}Al_2O_3$ catalyst. After the $Zn_{30}Cr_{4.5}/\gamma\text{-}Al_2O_3$ catalyst was used, the peak at 1450 cm^{-1} nearly disappeared, but it reappeared after regeneration. It therefore was concluded that the intermediate condensation of acrolein or propionaldehyde with

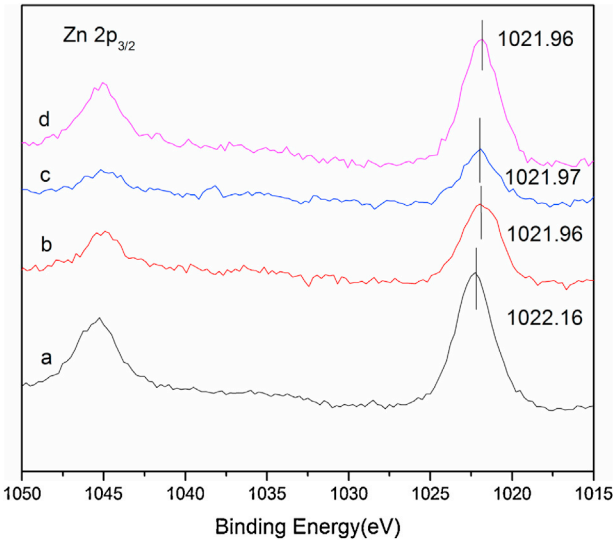

Fig. 3. Zn 2p and Cr 2p XPS spectra of the samples. (a) $Zn_{30}/\gamma\text{-}Al_2O_3$; (b) $Zn_{30}Cr_{4.5}/\gamma\text{-}Al_2O_3$ (Fresh); (c) $Zn_{30}Cr_{4.5}/\gamma\text{-}Al_2O_3$ (Used); (d) $Zn_{30}Cr_{4.5}/\gamma\text{-}Al_2O_3$ (Regenerated).

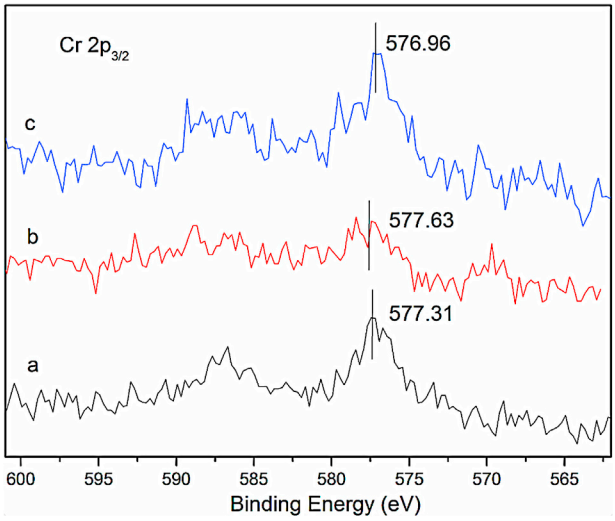

Fig. 4. High-resolution XPS spectra of $Zn_{30}Cr_{4.5}/\gamma\text{-}Al_2O_3$. (a) Fresh; (b) Used; (c) Regenerated.

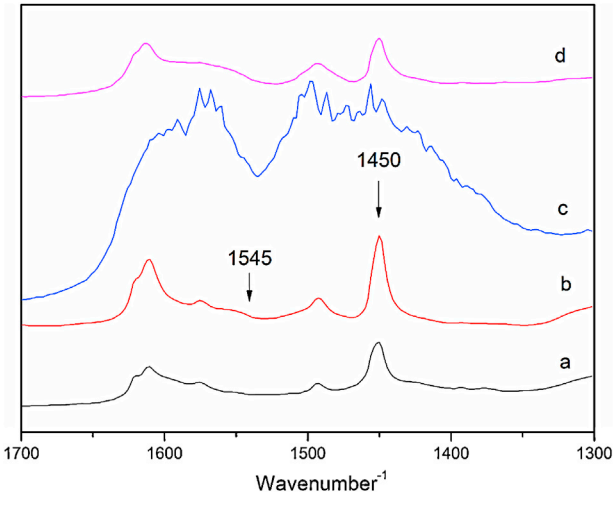

Fig. 5. IR spectra of pyridine adsorbed on the catalysts. (a) $Zn_{30}/\gamma\text{-}Al_2O_3$; (b) $Zn_{30}Cr_{4.5}/\gamma\text{-}Al_2O_3$ (Fresh); (c) $Zn_{30}Cr_{4.5}/\gamma\text{-}Al_2O_3$ (Used); (d) $Zn_{30}Cr_{4.5}/\gamma\text{-}Al_2O_3$ (Regenerated).

ammonia to form imines occurred on the Lewis acid sites of the catalyst. Obviously, an excess of ammonia over allyl alcohol impeded the reaction due to the adsorption of ammonia molecules on the acid sites. The disappearance of the peak at 1450 cm^{-1} in the spectrum of the used sample indicated that alkaline carbonaceous deposits were adsorbed on the Lewis acid sites and blocked the $ZnAl_2O_4$ active species, which led to the deactivation of the catalyst. After regeneration, the carbonaceous deposits were removed, and the acid sites and $ZnAl_2O_4$ active species were exposed to reactants again. Therefore, the activity of the catalyst was recovered.

4. Conclusions

A $Zn_{30}Cr_{4.5}/\gamma\text{-}Al_2O_3$ bimetallic catalyst was prepared and showed good performance for the amination of allyl alcohol to propionitrile. During the catalysis, the hydrogen generated during the dehydrogenation of the alcohol and imine acted as an in situ source for the hydrogenation of the carbon-carbon double bond. The parameters that affect the catalyst performance were studied thoroughly, and an optimized process for synthesizing propionitrile from allyl alcohol and ammonia over the catalyst was obtained. Under the optimized conditions, the propionitrile yield was greater than 65%. The characterization results indicated that the dehydrogenation reaction mainly occurred on the Lewis acid sites and revealed that $ZnAl_2O_4$ is the active species for the coupled dehydrogenation-hydrogenation reactions. Chromium doping of the $\gamma\text{-}Al_2O_3$-supported zinc catalyst $Zn_{30}/\gamma\text{-}Al_2O_3$ decreased the size of the $ZnAl_2O_4$ crystallites, which was favorable for the dehydrogenation–hydrogenation reactions. The characterization results also revealed that the catalyst deactivation was caused by carbon deposition on the catalyst during the catalytic run. The catalyst could be reactivated by blowing air into the reactor at a high temperature.

Acknowledgements

We thank the financial support of the National Natural Science Foundation of China (Grant no. 20976034), the Natural Science Foundation for Young Scientists of Hebei Province, China (Grant no. B2009000009) and the Foundation for Innovative Talents of Hebei Province, China (Grant no. CPRC012).

References

[1] S. Iida, H. Togo, Tetrahedron 63 (2007) 8274–8281.
[2] Y. Hu, J. Cao, J. Deng, B. Cui, M. Tan, J. Li, H. Zhang, React. Kinet. Catal. Lett. 106 (2012) 127–139.
[3] C. Feng, F. Guo, Y. Zhang, J. Zhao, Fine Chemicals (in Chinese) 27 (2010) 567–578.
[4] Y. Zhang, Y. Zhang, C. Feng, C. Qiu, Y. Wen, J. Zhao, Catal. Commun. 10 (2009) 1454–1458.
[5] C. Feng, Y. Zhang, Y. Zhang, Y. Wen, J. Zhao, Catal. Lett. 141 (2011) 168–177.
[6] D. Zhang, Y. Zhang, Y. Wen, K. Hou, J. Zhao, Chem. Eng. Res. Des. 89 (2011) 2147–2152.
[7] S.J. Kulkarni, R.R. Rao, M. Subrahmanyam, A.V.R. Rao, Appl. Catal. A 113 (1994) 1–7.
[8] K. Rajiv, J.P. Narahar, C.G. Moreshwar, N.P. Suresh, A. Ashutshot, V.P. Kumar, S.K. Samir, WO2005000816 (2005).
[9] Y. Zhang, W. Xu, J. Zhao, RSC Adv. 2 (2012) 6590–6598.
[10] F. Carey, R. Sundberg, Adv. Org. Chem., Springer US (2007) 63–214.
[11] A.J. Castro, D.K. Brain, H.D. Fisher, R.K. Fuller, J. Org. Chem. 19 (1954) 1444–1448.
[12] J.R. Calvin, R.D. Davis, C.H. McAteer, Appl. Catal. A 285 (2005) 1–23.
[13] Y. Higashio, T. Shoji, Appl. Catal. A 260 (2004) 251–259.
[14] J. Barrault, Y. Pouilloux, Catal. Today 37 (1997) 137–153.
[15] G. Lakshminarayana, L. Wondraczek, J. Solid State Chem. 184 (2011) 1931–1938.
[16] X. Duan, D. Yuan, Z. Sun, H. Sun, D. Xu, M. Lv, J. Cryst. Growth 252 (2003) 4–8.
[17] S. Farhadi, S. Panahandehjoo, Appl Catal. A 382 (2010) 293–302.
[18] H. Grabowska, M. Zawadzki, L. Syper, Appl. Catal. A 314 (2006) 226–232.

[19] J. Wrzyszcz, M. Zawadzki, J. Trawczyński, H. Grabowska, W. Miśta, Appl. Catal. A 210 (2001) 263–269.
[20] H. Grabowska, W. Miśta, J. Trawczyński, J. Wrzyszcz, M. Zawadzki, Appl. Catal. A 220 (2001) 207–213.
[21] H.H. Hng, P.L. Chan, Ceram. Int. 35 (2009) 409–413.
[22] Y. Wu, J. Du, K.-L. Choy, L.L. Hench, J. Guo, Thin Solid Films 472 (2005) 150–156.
[23] F. Simard, U.A. Sedran, J. Sepúlveda, N.S. Fígoli, H.I. de Lasa, Appl. Catal. A 125 (1995) 81–98.
[24] C.E. Volckmar, M. Bron, U. Bentrup, A. Martin, P. Claus, J. Catal. 261 (2009) 1–8.
[25] R. Barthos, F. Solymosi, J. Catal. 235 (2005) 60–68.
[26] E. Modrogan, M.H. Valkenberg, W.F. Hoelderich, J. Catal. 261 (2009) 177–187.